ACS APPLIED POLYMER MATERIALS

pubs.acs.org/acsapm Article

On the Formation Mechanism of Nonsolvent-Induced Porous Polylactide Electrospun Fibers

Yan-Ru Chen, Hsiao-Wei Chung, and Shih-Huang Tung*

Cite This: *ACS Appl. Polym. Mater.* 2021, 3, 5096−5104 Read Online

ACCESS | Metrics & More | Article Recommendations | Supporting Information

ABSTRACT: Polylactide (PLA) fibers were electrospun from the solutions of PLA dissolved in the mixtures of its good and poor solvents, and the formation mechanism of the poor solvent-induced porous structure on the fibers was investigated. From a systematic study using the pairs of a variety of good/poor solvents for electrospinning, the conditions, specifically the solvent properties, for producing uniform fibers with controllable pores that appear not only on the surface but also throughout the fibers were proposed. The water miscibility of the good/poor solvents is crucial, which is because the ambient moisture that condenses during electrospinning plays an important role in the formation of the pores. Furthermore, the evaporation rate of the good/poor solvents is another key factor that affects the pore size and pore distribution on fibers because the solvent evaporation rate regulates the moisture condensation and the phase-separated scale that are closely related to fiber morphology. The principles generalized in this work can be applied to other low-polar polymers for controlling the porosity of fibers. In addition, this work demonstrates that the porous PLA fibers can be electrospun from low-toxic solvents and that with a large surface area and storage space provided by the pores, the PLA porous fibers are highly capable of adsorbing oils, with a capacity double that of the smooth counterpart.

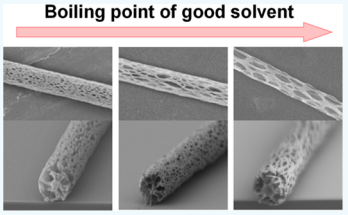

KEYWORDS: *polylactide, electrospinning, porous fibers, nonsolvent, oil adsorption*

INTRODUCTION

Electrospinning is a technique widely used to produce micro/nanoscale fibers with a large surface area.[1] To further increase the surface area, various methods have been developed to create porous structure on electrospun fibers, most by means of phase separation mechanisms analogous to those for fabricating porous polymer membranes.[2,3] The phase separation method involves the demixing of polymer solutions into polymer-rich domains and solvent-rich domains during electrospinning. After solvents fully evaporate, the solvent-rich domains leave vacancies on fibers. The major strategies to cause demixing of solutions include thermally induced phase separation (TIPS), vapor-induced phase separation (VIPS), and nonsolvent (or poor solvent)-induced phase separation (NIPS). For the TIPS method, the homogeneous polymer solution in the electrospun jet is rapidly cooled, which turns the solvent to be poorer to the polymer and causes a phase separation.[4] The temperature difference can be achieved by controlling the solution at a relatively high temperature[5] or the fiber collector at a relatively low temperature.[6] VIPS requires solvents with low volatility and high water miscibility. The ambient water vapor is condensed upon solvent evaporation, and the condensed water that dissolves in solutions serves as the nonsolvent, causing originally homogeneous solutions to phase-separate.[7−11] In NIPS, the phase separation is induced by nonsolvents (or poor solvents) that are intentionally incorporated into polymer solutions. This is carried out either by immersing liquid jets into nonsolvent baths during electrospinning[12−14] or by premixing lower volatile nonsolvents to form homogeneous polymer/good solvent/nonsolvent ternary solutions.[15−21] In the latter case, the nonsolvent fraction gradually increases to trigger demixing due to faster evaporation of the good solvent during electrospinning. In addition to the phase separation mechanisms, other methods to create porosity for electrospun fibers include the breath figure (BF) process that gives pores only on the fiber surface,[22−25] selective removal of one component from blended fibers,[26−29] and direct printing patterns on fibers by porous templates.[30]

The electrospinning from the premixed polymer/good solvent/nonsolvent ternary solutions (NIPS) can obtain highly porous fibers and can be accomplished by a simple one-step process without the requirement of post-treatments. Although the addition of nonsolvents or poor solvents into polymer solutions can induce phase separation that causes porosity, the fiber diameter and the pore size of the fibers electrospun from most of the ternary systems are uneven.[16−18,20] This implies that the component and composition of the ternary solutions require an optimization to acquire uniform porous fibers. In

Received: July 14, 2021
Published: September 3, 2021

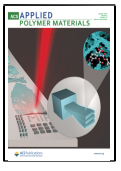

https://doi.org/10.1021/acsapm.1c00855
ACS Appl. Polym. Mater. 2021, 3, 5096−5104

our previous report, the solution of polystyrene (PS) dissolved in cosolvents composed of a good solvent chlorobenzene (CB) and a nonsolvent dimethyl sulfoxide (DMSO) can be electrospun into macroporous fibers with a uniform fiber size.[31] More importantly, the porous structure not only appears on the surface but also appears throughout the fibers, which drastically increases the surface area.[32] The fiber size and the pore morphology can be tuned by changing the compositions of the polymer solutions. These PS fibrous sorbents with superhydrophobic properties can selectively adsorb oils while repel water and show an exceptional oil adsorption capability. Despite successful preparation of the uniform highly porous fibers, the reason why the PS/CB/DMSO system works well while others do not is not fully understood.

Polylactide (PLA) is an environmentally friendly, biodegradable, and biocompatible polyester synthesized from renewable feedstocks. Because of these attractive characteristics, PLA electrospun fibers have been widely studied and various methods have been implemented to increase porosity, including the NIPS,[15,17,20,23,33] VIPS,[15] BF,[15,23,25] and blending/removal[27] methods, among which NIPS is the most popular method. The applications of the porous PLA fibers are diverse, ranging from oil adsorption and separation[34−39] and aerosol filtration[40] to cartilage regeneration.[41] However, for the PLA porous electrospun fibers prepared by the NISP method in previous reports, the fiber morphologies varied from one another as different good/poor solvents were used. The mechanisms were thus provided on a case-by-case basis.

In this work, PLA was used as the model polymer to clarify the mechanism for the formation of porous electrospun fibers by the NIPS method. PLA ternary solutions were prepared with pairs of a variety of good/poor solvents. The effects of the water miscibility, evaporation rates, and polarities of the good/poor solvents on fiber morphology were systematically investigated. The effect of ambient moisture was also studied. By a careful examination, the conditions for fabricating uniform porous fibers were proposed. The results suggest that a mechanism combining VIPS and NIPS coupled with the optimized component and composition in the cosolvent is required. More specifically, the condensed water during electrospinning needs to be highly miscible with the poor solvents to promote demixing and there must be enough time for the liquid−liquid phase separation to grow into polymer-rich and highly solvent-rich domains. While most of the good solvents that can work are halogenated or highly toxic, such as CB and benzene (BZ), the porous fibers were successfully prepared from a low-toxic PLA/ethyl acetate (EA)/DMSO system, manifesting that the green and sustainable PLA porous fibers can be processed in an eco-friendly manner. Moreover, the sorbents made by the PLA porous fibers show a high oil adsorption capacity, up to 800 g/g for high viscous oils, due to a significant increase in the surface area provided by the pores.

EXPERIMENTAL SECTION

Materials. PLA (M_n = 118,190 g/mol and PDI = 1.67) was purchased from NatureWorks. Tetrabutylammonium perchlorate (TBAP, >98%) was purchased from TCI. The solvents used in this work all met the ACS reagent grade specifications. The abbreviations of the solvents used in this work are shown in Table 1, and their physical properties are listed in Tables S1 and S2 of Supporting Information and in Table 2. All chemicals were used as received, and the solvents were carefully stored in a desiccator to prevent absorption of water.

Table 1. Good/Poor Solvents and Their Abbreviations Used in This Work

Good Solvent	
BZ: benzene	EA: ethyl acetate
CB: chlorobenzene	NMP: N-methylpyrrolidone
CF: chloroform	TCE: 1,1,2,2-tetrachloroethane
DCM: dichloromethane	THF: tetrahydrofuran
DO: 1,4-dioxane	
Poor Solvent	
AA: acetic acid	DMF: *N*,*N*-dimethylformamide
AN: anisole	DMSO: dimethyl sulfoxide
BA: butyl acetate	ET: ethanol
BT: 1-butanol	MEK: methyl ethyl ketone
CH: cyclohexane	MIBK: methyl isobutyl ketone
DCB: *o*-dichlorobenzene	MT: methanol
DE: *n*-decane	OT: 1-octanol
DEA: *N*,*N*-diethylacetamide	PP: 1-propanol
DEF: *N*,*N*-diethylformamide	TL: toluene
DMA: *N*,*N*-dimethylacetamide	XL: *o*-xylene

Electrospinning Process. PLA was mixed in cosolvents of various good solvents and poor solvents at different ratios, with or without 1.5% (w/v) TBAP, to prepare PLA solutions for electrospinning. The concentration of PLA is 150 mg/mL, unless otherwise specified. The addition of TBAP was to increase the conductivity of the solutions. The mixtures were magnetically stirred until homogeneous solutions were reached. The electrospinning was conducted using a single-capillary spinneret. The PLA solutions were fed into a syringe pump (YSP-101, YMC) connected to a metallic needle (22 gauge, Hamilton) at a feed rate of 0.5 mL/h. A power supply (chargemaster VCM30-P, Simco-Ion) was connected to the metallic needle to provide the voltage for ejecting the PLA solutions. The applied voltage was 7.2−12 kV. The fibers were collected on a piece of aluminum foil placed 15 cm below the tip of the needle. The experiments were carried out at room temperature (22−26 °C) and a relative humidity (RH) of 50−70%, unless otherwise specified.

Scanning Electron Microscopy. The morphologies of fibers were characterized using a JEOL JSM-6330F field-emission scanning electron microscopy (SEM) instrument at an accelerating voltage of 3−5 kV. Before imaging, the samples were sputtered with platinum. For probing the cross-sectional structures, the fibers were first transferred onto silicon wafer and sputtered with platinum. After sputtering, the wafer was cut into two pieces in the liquid nitrogen, which simultaneously fractured the fibers attached on the wafer to reveal the fiber cross sections for imaging.

Phase Diagram of Solutions. A series of solutions with varying compositions of PLA, CB, and DMSO were sealed in glass bottles. The mixtures were first heated up to 80 °C and stirred until the solutions became homogeneous and transparent. The solutions were then cooled to room temperature. The liquid−liquid demixing boundary at room temperature was determined by the cloud point method. The solutions remaining transparent were stable, while those turning to be cloudy were in the unstable regime where liquid−liquid demixing occurred.

Mercury Intrusion Porosimetry. The pore size distributions of fibrous mats were determined using a mercury porosimeter (AutoPore IV 9520, Micromeritics). The applied pressure (P) ranged from 0.1 to 60,000 psia, and samples were equilibrated at each pressure for 15 s. The pressure was converted to the pore diameter (D) by assuming the cylindrical pore geometry using the Washburn equation[42]

$$D = \frac{-4\gamma \cos\theta}{P} \quad (1)$$

https://doi.org/10.1021/acsapm.1c00855
ACS Appl. Polym. Mater. 2021, 3, 5096−5104

Table 2. Solvent Properties and the Pore Size on the Fiber Surface Using Varying Pairs of the Good/Poor Solvents

			good solv.	THF	DO	NMP	DCM	CF	EA	BZ	CB	TCE
			T_b[a] (°C)	66	101	202	40	61	77	80	131	147
			ε[b]	7.58	2.25	32.2	8.93	4.81	6.02	2.27	5.62	8.42
poor solv.	T_b (°C)	ε	water misc.[c]	○	○	○	×	×	Δ	×	×	×
CH	81	2.02	×									
TL	111	2.38	×									
BA	126	5.10	×									
XL	144	2.57	×									
MIBK	116	13.1	×									
AN	155	4.33	×									
DCB	174	9.93	×									
DE	174	2.00	×									
OT	195	10.3	×									
MT	65	32.7	○									
ET	78	24.5	○									
MEK	80	18.5	○									
PP	97	20.1	○									
BT	118	17.8	Δ									
AA	118	6.15	○									
DMF	153	36.7	○				small	small	small	medium	large	
DMA	165	37.8	○				small	small	small	medium	large	
DEF	177	29.0	○									
DEA	184	31.3	○									
DMSO	189	46.7	○				small	small	medium	medium	large	large

[a]Boiling point. [b]Dielectric constant. [c]water miscibility (○ high, Δ medium, and × low).

where the surface tension (γ) of mercury is 485 dyn/cm and a contact angle (θ) of 130° was used. The volumes of pores at the corresponding sizes were measured based on the volume of the intruded mercury. The cumulative specific intrusion volume (V) of mercury as a function of D was first determined. The pore size distribution curve is expressed as dV/dD against D. The porosity and the total surface area of the samples were also determined by mercury intrusion porosimetry.

Oil Adsorption Tests. The oil adsorption capacities of fibers were measured as follows. The fibers were gently removed from the aluminum foil collectors with slow air blowing to prevent the as-spun format of the fibers from damage. Approximately 10 mg of fibrous sorbents was immersed in oils in a glass beaker. After 1 h of adsorption, the sorbents were removed from the oil bath and drained for 1 min. The oil adsorption Q (g/g) of the fibers is determined by

$$Q = \frac{w - w_0}{w_0} \quad (2)$$

where w is the total weight of the sorbent after adsorption and draining and w_0 is the weight of the sorbent before adsorption. Each sample was independently measured for at least five times.

RESULTS AND DISCUSSION

The electrospun fibers are named based on the compositions of the solutions. Taking CB-DMSO15-T as an example, CB is the good solvent, DMSO is the poor solvent and its volume fraction is 15% of the total solvent, and T represents the addition of 1.5% (w/v) TBAP in the solvent. PLA is a semicrystalline polymer. The electrospun PLA fibers, however, are nearly amorphous due to the rapid evaporation of solvents during electrospinning, which is evidenced by the differential scanning calorimetry (DSC) thermogram that shows equal recrystallization and melting heats (Figure S1). The effect of the crystallinity on the fiber morphology is thus ruled out.

Water Miscibility of Solvents. The solvent effects on the pore formation of the electrospun fibers are first discussed. Our previous report has shown that a cosolvent composed of proper good and poor solvents to the polymer is required to fabricate the macroporous fibers.[31] A liquid−liquid phase separation must occur during the electrospinning process to create pores. However, not all the good/poor solvent pairs can give the same result. To clarify the mechanism, PLA fibers were electrospun using different pairs of good and poor solvents with varying water miscibility, evaporation rate, and polarity. All the solvents used in this work are listed in Tables 1 and 2. The water miscibility of the solvents on the pore formation was first examined as follows. The RH was about 60% for this test.

Water-Miscible Good and Poor Solvents. The SEM images of the representative fibers electrospun from the pairs of good and poor solvents that are both water-miscible are shown in Figure S2. The water-miscible good solvents include THF, DO, and NMP, and the poor solvents include ET, BT, AA, DMA, and DMSO. No pores are formed on the fiber surface, and only some small dents are found for the poor solvents with high boiling points (T_b), such as DMA and DMSO.

Water-Miscible Good Solvents and Water-Immiscible Poor Solvents. Figure S3 shows the representative fibers electrospun from the water-miscible good solvents, including THF, DO, and NMP, and the water-immiscible poor solvents, including CH, TL, BA, XL, AN, and DCB. These solvent pairs are unable to cause pore formation, and only some wrinkles are formed on the surface of the fibers.

Water-Immiscible Good and Poor Solvents. In the representative cases combining water-immiscible good solvents, including CF, BZ, CB, and TCE, with water-immiscible poor solvents, including TL, XL, AN, DCB, and OT, only small pores can be found on fibers using the good solvents of lower T_b, such as CF and BZ, as shown in Figure S4. The others are smooth. The cross-sectional SEM images of the fibers with small pores reveal that the pores only appear on the surface and the fiber interiors remain solid. The formation of

https://doi.org/10.1021/acsapm.1c00855
ACS Appl. Polym. Mater. 2021, 3, 5096−5104

the surface pores is due to the rapid evaporation of the low-T_b solvents that causes the condensation of the water drops on the liquid surface before solidification, that is, a BF phenomenon.[22]

Water-Immiscible Good Solvents and Water-Miscible Poor Solvents. The morphologies of the representative fibers electrospun from the pairs of the water-immiscible good solvents, including DCM, CF, BZ, CB, and TCE, and the water-miscible poor solvents, including PP, DMA, DEA, and DMSO, are shown in Figure 1. Porous fibers can be produced

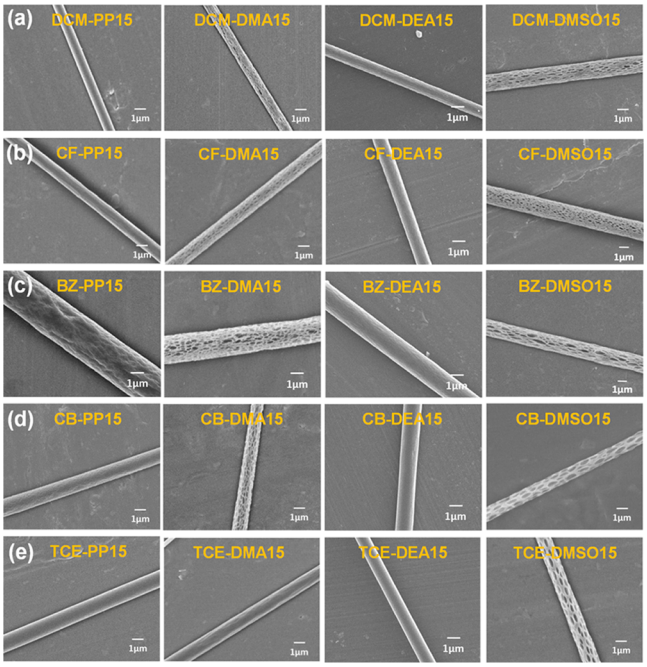

Figure 1. SEM micrographs of the fibers electrospun from water-immiscible good and water-miscible poor solvents: good solvents (a) DCM, (b) CF, (c) BZ, (d) CB, and (e) TCE paired with poor solvents PP, DMA, DEA, and DMSO.

using high-T_b DMA and DMSO as the poor solvents, except the combination of DMA paired with the high-T_b good solvent TCE. The pore size on the surface increases with increasing T_b of the good solvents, which can be seen by comparing the fibers on the rightmost column in Figure 1 using DMSO as the poor solvent. The large pores are elongated along the fiber axis due to the stretching force caused by electrospinning. Moreover, the pores not only appear on the surface but also extend into the core of the fibers, as evidenced by the cross-sectional SEM images of the fibers with DMSO in Figure 2. For the fibers using low-T_b DCM and CF as the good solvents, the voids inside the fibers are large even though the pores on the surface are small. Note that although the T_b of DEA is between those of DMA and DMSO, the use of DEA as the poor solvent is unable to fabricate porous fibers. As shown in Table 2, the dielectric constant (ε) of DEA is lower than those of DMA and DMSO. It is apparent that the highly porous fibers can only be electrospun from the pairs of water-immiscible good solvents and water-miscible poor solvents under some specific conditions related to T_b and ε of the solvents. The effects of T_b and ε which correlate with the evaporation rates and polarities of solvents are discussed in the following sections.

Humidity Effect. As the solvents evaporate to withdraw heat and lower the temperature during electrospinning, the

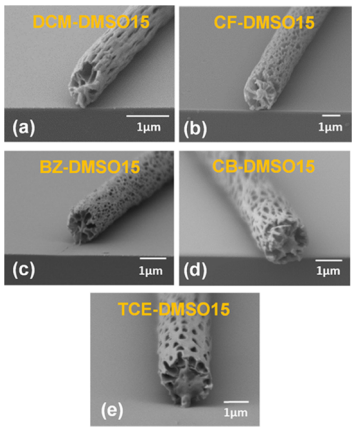

Figure 2. SEM cross-sectional micrographs of the porous fibers electrospun from the poor solvent DMSO paired with the good solvents of varying T_b from low to high: (a) DCM, (b) CF, (c) BZ, (d) CB, and (e) TCE.

ambient moisture condenses on the liquid jets. Because water is a nonsolvent to PLA, the effect of the humidity should be considered. Figure 3 shows the SEM images of the PLA fibers

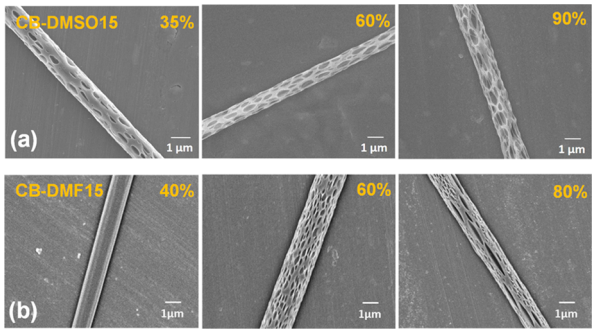

Figure 3. SEM micrographs of (a) CB-DMSO15 and (b) CB-DMF15 fibers electrospun at varying relative humidity.

electrospun at varying RH from the CB/DMSO and CB/DMF solutions that can successfully create pores. For the CB/DMSO system, fewer and smaller pores are formed at 35% RH. The size of the pores increases and the shape of pores is elongated along the fiber axis with increasing humidity. For the CB/DMF system, small pores are formed at 60% and they merge into elongated slits at 80% RH, whereas the fibers are smooth at 40% RH. The results manifest the crucial role of the ambient moisture in the pore formation. To mimic the absorption of water into the liquid jets during the electrospinning process, we intentionally added 1 wt % of water into the PLA/CB/DMSO solution. The phase diagram is shown in Figure S5. The black solid curve is the original phase-separation boundary without water. The boundary expands to the blue dashed curve in the presence of 1 wt % water. In other words, water can facilitate the liquid−liquid phase separation of the PLA solutions, which is favorable for the pore formation.

Water miscibility of solvents matters as described in the preceding section because it affects the liquid−liquid phase separation process. If the condensed water is immiscible with both the good solvent and poor solvent, water drops can only locate on the surface of liquid jets and leave small, shallow pores after the solvents are dried, that is, the BF process, especially for the low-T_b good solvents that rapidly evaporate,

https://doi.org/10.1021/acsapm.1c00855
ACS Appl. Polym. Mater. 2021, 3, 5096−5104

as shown in Figure S4. If the condensed water is miscible with the poor solvent but not with the good solvent, the solvent quality of the poor solvent combining water becomes even poorer to PLA, which promotes demixing to form a highly solvent-rich phase with nearly the poor solvent and condensed water and a polymer-rich phase with PLA dissolved in the good solvent in a short time. The highly solvent-rich phase can then lead to the pores after the solvents are dried. However, if the condensed water is miscible with both the good solvent and poor solvent or only miscible with the good solvent but not with the poor solvent, the highly solvent-rich phase that causes the well-defined pores is unable to form during electrospinning even though a small-scale phase separation may still occur.

As shown in Figure 1, while the use of high-T_b DMA and DMSO as poor solvents can fabricate porous fibers, the high-T_b DEA is unable to make the pores. Although DEA is a water-miscible poor solvent, the polarity of DEA is lower than those of DMA and DMSO, which is reflected by the lower ε of DEA, as shown in Table 2. Water prefers to mix with high-polar solvents, and thus, the diffusion rates of water and DEA molecules to intermix are slower than those in the DMA and DMSO cases. Because the electrospinning process is completed in a very short time, if there is not enough time for the condensed water to homogeneously mix with poor solvents to promote the liquid−liquid phase separation, the pores are hardly formed. This explains why the use of low-ε DEA can only produce smooth fibers, which is also true for low-ε DEF as the poor solvent, as shown in Table 2.

Evaporation Rates of Solvents. In addition to the use of water-immiscible good solvents with water-miscible poor solvents, the T_bs of the solvents play a role in the formation of the pores. T_b is an indication of the solvent evaporation rate, and in general, the higher the T_b, the lower the evaporation rate is. The difference in evaporation rates of the good solvent and poor solvent causes the composition change in the liquid jet during electrospinning, which in turn affects the phase separation process. As shown in Figure 1, only the poor solvents with high T_b, such as DMA and DMSO, can give rise to pores. When T_b of the good solvents increases, the pore size on the fiber surface increases. However, when T_b of the good solvent is close to that of the poor solvent, such as the TCE (147 °C)/DMA (165 °C) pair, the pores are unable to form, which also explains why the pores are absent for the fibers with low-T_b poor solvents, such as PP (Figure 1). In other words, to create pores, T_b of the poor solvent must be significantly higher than that of the good solvent. The more rapid evaporation of good solvents leads to an increasing fraction of poor solvents in the liquid jets, which triggers the liquid−liquid phase separation at an earlier stage, along with the condensed water that mixes in the poor solvents. There is thus enough time for the separation to proceed and create the pores during electrospinning. As the evaporation rates of good solvents are comparable to or even higher than those of poor solvents, the solvent composition is not significantly changed or even becomes favorable to PLA during electrospinning. The fiber is thus smooth, like those electrospun from neat good solvents. Note that for the low-T_b good solvents, such as DCM, CF, and BZ, the fast evaporation of the good solvents results in a low fraction of the good solvent on the surface and causes an earlier solidification of PLA to form a denser skin, which is why the pores on the surface are smaller than the voids inside the fibers where large-scale liquid−liquid phase separation remains active.

Mechanism. As summarized in Table 2, the uniform porous fibers can be successfully electrospun only with limited pairs of good/poor solvents, among which the pore size on the surface can be controlled by varying the good solvents. Based on the results, we propose the conditions for the formation of uniform porous fibers: (1) the good solvent must be water-immiscible, (2) the poor solvent must be water-miscible and have a high polarity (ε > 35), and (3) T_b of the poor solvent must be at least 20 °C higher than that of the good solvent. These conditions fulfill the following mechanism to create pores on fibers. First, the high-polar poor solvent can increase the polarizability of the solutions, which facilitates electrospinning. During the electrospinning process, the liquid jet upon ejection is homogeneous initially, and then, solvent evaporation, moisture condensation, and phase separation occur in a very short time. In the liquid jets, the lower-T_b good solvent evaporates faster to condense moisture that can homogeneously mix with the higher-T_b poor solvent to promote phase separation. The solution in the liquid jet then rapidly phase-separates into the highly solvent-rich phases containing mostly the poor solvent and water, and the polymer-rich phases containing mostly the good solvent and polymer. The phase separation initiates on the surface and then propagates into the interior of the liquid jet with time. The elongation of the large pores along the fiber axis indicates that the phase separation occurs prior to polymer solidification. When the solvents are dried out, the polymer-rich phase solidifies first due to a higher evaporation rate and the highly solvent-rich phase forms the well-defined pores that extend from the surface into the fibers. The process is illustrated in Figure 4. The good solvent with higher T_b evaporates slowly,

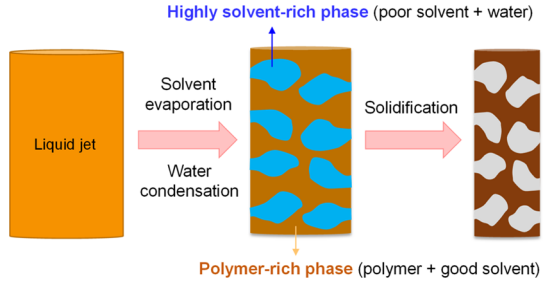

Figure 4. Schematic of the formation mechanism of porous fibers during electrospinning.

which allows more time for the phase-separated domains to grow on the surface so that the pore size on the surface is larger (Figure 1 and Table 2). In addition to PLA, the abovementioned mechanism can be applied to other low-polar polymers for fabricating porous fibers, such as PS[31] and poly(methyl methacrylate) (PMMA) (Figure S6).

Morphology. Here, we use the PLA/CB/DMSO system to investigate the effect of the poor solvent fraction and the effect of the extra salt TBAP that is added to increase the polarizability of solutions. The SEM images of the representative fibers and their cross sections are shown in Figure 5a, and the fiber sizes are listed in Table 3. The CB-DMSO0-T fibers electrospun from 100% good solvent CB with the addition of 1.5% (w/v) TBAP are smooth on the surface and are solid inside. Note that the solution of PLA and pure CB cannot be successfully electrospun into fibers due to low polarizability of the solution, which is why TBAP is required to enhance electrospinnability for fabricating CB-

https://doi.org/10.1021/acsapm.1c00855
ACS Appl. Polym. Mater. 2021, 3, 5096−5104

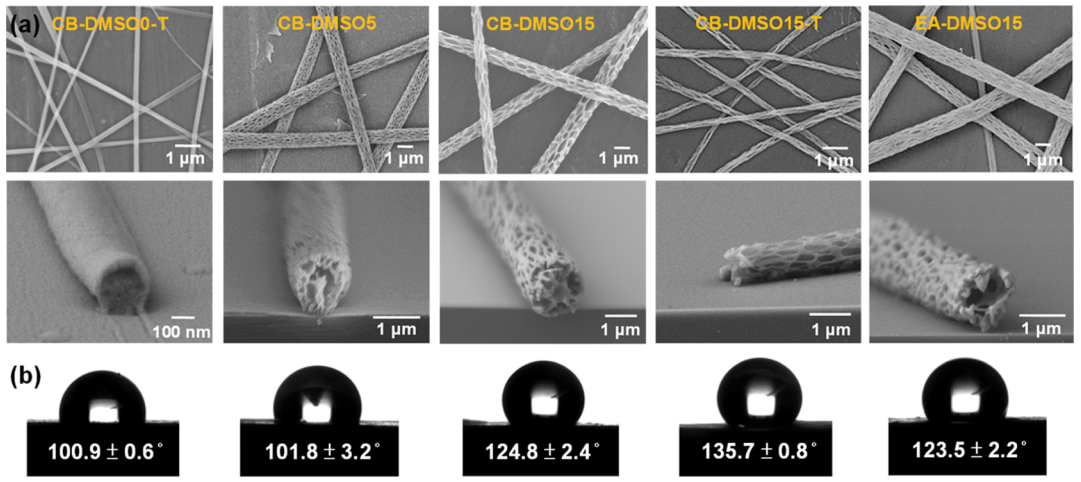

Figure 5. (a) SEM micrographs of five representative fibers electrospun from PLA/CB/DMSO and PLA/EA/DMSO systems. (b) Images of the water droplets and the averaged contact angles on the surface of the fibrous mats.

Table 3. Characteristics of the Fibrous Mats Shown in Figure 5

fiber	diameter (μm)	porosity (%)	total surface area (m^2/g)
CB-DMSO0-T	0.29 ± 0.12	91.4	39.6
CB-DMSO5	1.03 ± 0.26	89.8	16.6
CB-DMSO15	1.03 ± 0.23	91.2	21.1
CB-DMSO15-T	0.31 ± 0.08	91.7	44.6
EA-DMSO15	1.06 ± 0.26	88.4	40.0

DMSO0-T fibers. The CB-DMSO5 and CB-DMSO15 fibers with the poor solvent involved are porous, both on the surface and in the interior, and the size of the pores increases with increasing DMSO fraction. The dependence of the pore size on the DMSO fraction can be more clearly seen in Figure S7 where the SEM images of the fibers electrospun with 5−20% DMSO are compared. The addition of TBAP can significantly reduce the fiber diameter. Without TBAP, the fiber diameter is ~1000 nm on average and it decreases to ~300 nm in the presence of TBAP, as evidenced by the CB-DMSO15-T and CB-DMSO0-T fibers.

In Table 2, the good solvents that can be used to fabricate porous fibers are mostly halogenated or toxic solvents, which may raise environmental and health concerns. Among the good solvents, EA is low toxic and can serve as the good solvent to produce porous fibers. T_b of EA is sufficiently high (77 °C) and the water miscibility of EA is sufficiently low to fulfill the requirements of the good solvent. When paired with DMSO as the poor solvent, the EA-DMSO15 fibers form middle-size pores on the surface and large voids in the interior, as shown in Figure 5. In other words, the eco-friendly porous PLA fibers can be electrospun through a green process. The pore size of the EA-DMSO15 fibers on the fiber surface is not as large as that of the CB-DMSO15 fibers because the T_b of EA is lower, which limits the growth of the solvent-rich phases on the surface due to earlier polymer solidification. The earlier PLA solidification causes a robust, fixed skin inside which the phase-separated domains keep growing, thus leaving the large voids inside the fibers after drying.

The mercury porosimeter was used to determine the pore sizes of the fibers. Figure 6 shows the pore size distribution of the fibrous mats displayed in Figure 5. In the fibrous mats, there are two possible spaces that can be filled with mercury

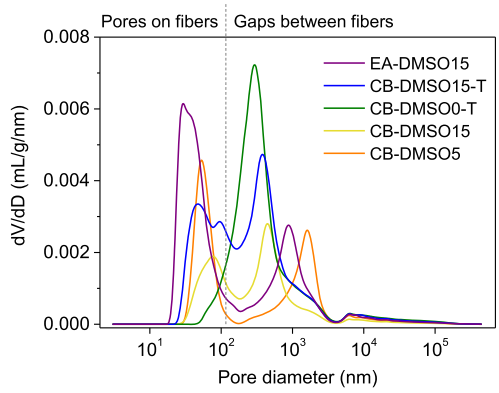

Figure 6. Pore size distributions of the fiber mats shown in Figure 5 determined using a mercury porosimeter.

under pressure: one from the gaps between the fibers and the other from the pores on the fibers. Except that the CB-DMSO0-T fibers show only one distribution of pore size between 100 and 1000 nm, other fibers exhibit two major distributions, a small one between 10 and 100 nm and a large one between 100 and 10,000 nm. The size larger than 100 nm can be rationally attributed to the gaps between fibers in the mats, while the size smaller than 100 nm is given by the pores on the fibers. Because the CB-DMSO0-T fibers are smooth, only can the interfiber gaps be measured. For the porous fibrous mats, as expected, the signals of the pores on fibers appear in addition to the interfiber gaps. The pore size is in the order CB-DMSO15 > CB-DMSO5 > EA-DMSO15, which agrees with the trends found in the SEM images of Figure 5a. The pore size of the CB-DMSO15-T fibers splits into two distributions with an average approximate to that of the CB-DMSO15 fibers. Note that the size of the interfiber gap is positively related to the diameters of the fibers. For the thinner fibers, including CB-DMSO0-T and CB-DMSO15-T electrospun with TBAP, the sizes of the interfiber gaps are smaller than those of the thicker fibers without TBAP. This is possibly because thinner fibers can more closely stack to narrow the gaps in the mats.

The porosities and the total surface areas of the fibrous mats determined using the mercury porosimetry are listed in Table 3. The porosities of all the fibrous mats are similar, as high as

https://doi.org/10.1021/acsapm.1c00855
ACS Appl. Polym. Mater. 2021, 3, 5096−5104

90%. The total surface areas of the fibrous mats are in the order CB-DMSO15-T > EA-DMSO15 > CB-DMSO0-T > CB-DMSO15 > CB-DMSO5. The thin, macroporous CB-DMSO15-T shows a high surface area of up to 44.5 m^2/g, and those of EA-DMSO15 with large interior voids and the thin, smooth CB-DMSO0-T are around 40 m^2/g. The thick fibers show lower surface areas, 21.1 and 16.6 m^2/g for CB-DMSO15 of larger pores and CB-DMSO5 of smaller pores, respectively. The total surface area is related to the oil adsorption capacity, as will be discussed later.

The hydrophobicities of the fibrous mats were evaluated by the measurement of the water contact angle (WCA), as shown in Figure 5b. The WCA of the spin-cast pure PLA film is 76.0°. Because the interfiber gap can reduce the direct water−solid contact to enhance hydrophobicity, the WCA of the thin, smooth CB-DMSO0-T mat increases to 100.9°. With pores on fibers, the WCA further increases. The WCA of the thick CB-DMSO5 fibers with small pores slightly increases to 101.8°, while those of the thick CB-DMSO15 and EA-DMSO15 fibers with larger pores greatly increase to 124.8°. The thin CB-DMSO15-T fibers with large pores show the highest WCA of 135.7°. The WCAs of thin fibers are higher than those of thicker fibers because the interfiber gaps of the thinner fibers are smaller and can more efficiently trap air between water drops and the mats, thus preventing water from wetting on the mat surface. Furthermore, the porous structure on fibers can significantly increase the WCA because the surface roughness makes extra contribution to the hydrophobicity. Such a property is advantageous for the porous fibers used as the lipophilic sorbents for separating oils from water.

Oil Adsorption Capacity. The five representative fibers shown in Figure 5 were used as sorbents to assess the adsorption capability for various oils. Due to the hydrophobic nature of PLA fibers, the fibrous mats can selectively adsorb oil while repel water. The oil adsorption capacities of the fibers with five different oils are shown in Figure 7. Overall, the

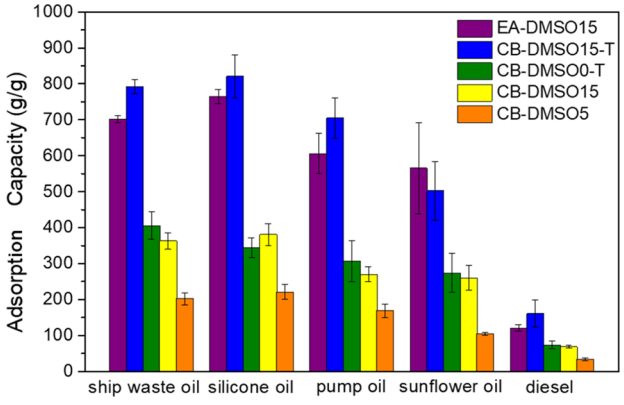

Figure 7. Maximum oil adsorption capacities of the fibrous sorbents for different oils.

amount of the oils adsorbed by the sorbents is positively related to the viscosity of oils, following the order: ship waste oil > silicone oil (1.021 Pa·s) > pump oil (0.143 Pa·s) > sunflower oil (0.054 Pa·s) > diesel (0.004 Pa·s). Note that the waste oil from ships is a colloidal solution that exhibits non-Newtonian flow properties with the highest viscosity at rest. Such a viscosity dependence is because the higher viscous oils can adhere more firmly in the fibers and flow slower to avoid draining after adsorption. Comparing the oil adsorption of the five fibers, the capacity is in the order CB-DMSO15-T > EA-DMSO15 > CB-DMSO0-T > CB-DMSO15 > CB-DMSO5. The adsorption capacities of the thin, porous CB-DMSO15-T fibers for the silicone oil and ship waste oil are up to 800 g/g, and those of the EA-DMSO15 fibers fabricated by low-toxic solvents are above 700 g/g. The samples were noticeably swollen after adsorption due to a large volume of oils trapped in the mats.

The order of the oil adsorption capacity of the fibers approximately follows the order of the total surface area shown in Table 3, highlighting the role of the surface area in oil adsorption. The oil adsorption is driven by capillary forces, and the adsorbed oils are distributed both in the gaps between fibers and the pores on the fibers. Thinner fibers show higher adsorption capacities because the thinner fibers provide more surface area that can adhere to oils so that the oils can be more effectively retained in the interfiber gaps. The porous structure on fibers further contributes space to accommodate oils and provides the surface area to retain oils, thus enhancing adsorption capacity. This explains why the thin CB-DMSO15-T fibers with large pores show the highest adsorption capacity. The adsorption capacity of the thin, smooth CB-DMSO0-T is slightly higher than that of the thick, macroporous CB-DMSO15, and the thick CB-DMSO5 fibers with small pores show the lowest capacity. By comparing the fibers with a similar diameter, CB-DMSO15-T and CB-DMSO0-T, the adsorption capacity of the porous fibers is found to be about twice that of the smooth ones. Although the EA-DMSO15 fibers are thick and the pore size on the fiber surface is smaller, the large voids inside the fibers and the large surface area can effectively store oils. The EA-DMSO15 fibers therefore show a superior oil adsorption capacity, only second to the CB-DMSO15-T fibers.

The adsorption capacities of PLA fibers in the previous reports are generally in the range between 100 and 200 g/g,[15,43] which are lower than the values obtained in this work. Note that the sorbent compactness that depends on the ways to collect fibers and to remove the fibrous mats from the substrate after electrospinning may greatly affect the adsorption capacity. Compared to the PS fibers prepared by a similar method in our previous report where the adsorption capacity of the PS porous fibers is up to 900 g/g for silicon oil,[31] the capacity of the PLA porous fibers is slightly lower. This is mainly because PLA is more hydrophilic than PS in nature. The oil-PLA affinity is thus relatively lower due to the higher attractive force between PLA fibers.

CONCLUSIONS

In this work, the conditions for fabricating uniform porous fibers electrospun from the solution of PLA dissolved in mixtures of good and poor solvents were systematically studied. During the electrospinning process, various phenomena, including solvent evaporation, moisture condensation, phase separation, and polymer solidification, occur in a very short time. This complexity requires a proper coordination of the solvent polarity and evaporation rate to create porous fibers. Regarding the solvent polarity, the good solvent must be water-immiscible, and the poor solvent must be water-miscible and highly polar. The evaporation rate of a solvent is closely related to its T_b. The T_b of the poor solvent must be sufficiently higher than that of the good solvent, and the higher the T_b of the good solvent, the larger the pores on the fiber surface are. While PLA is used as the model polymer in this

https://doi.org/10.1021/acsapm.1c00855
ACS Appl. Polym. Mater. 2021, 3, 5096−5104

work, the principles found in this work can be applied to other low-polar polymers, such as PS and PMMA. The porous PLA fibers can work as efficient oil sorbents that show an adsorption capacity as high as 800 g/g. Furthermore, the porous PLA fibers can be electrospun from the low toxic solvents, one example being the pair of EA and DMSO. Because PLA is a biocompatible polymer, the highly porous PLA fibers are also potential for applications in the biomedical field.

■ ASSOCIATED CONTENT

Supporting Information

The Supporting Information is available free of charge at https://pubs.acs.org/doi/10.1021/acsapm.1c00855.

Properties of good and poor solvents, DSC thermogram of PLA electrospun fibers, phase diagram of the PLA/CB/DMSO ternary system, SEM micrographs of PS and PMMA fibers, and additional SEM micrographs of PLA fibers (PDF)

■ AUTHOR INFORMATION

Corresponding Author

Shih-Huang Tung − *Institute of Polymer Science and Engineering and Advanced Research Center for Green Materials Science and Technology, Naional Taiwan University, Taipei 10617, Taiwan;* orcid.org/0000-0002-6787-4955; Email: shtung@ntu.edu.tw

Authors

Yan-Ru Chen − *Institute of Polymer Science and Engineering, National Taiwan University, Taipei 10617, Taiwan*

Hsiao-Wei Chung − *Institute of Polymer Science and Engineering, National Taiwan University, Taipei 10617, Taiwan*

Complete contact information is available at: https://pubs.acs.org/10.1021/acsapm.1c00855

Notes

The authors declare no competing financial interest.

■ ACKNOWLEDGMENTS

This work was financially supported in part by the "Advanced Research Center of Green Materials Science and Technology" from the Featured Area Research Center Program within the framework of the Higher Education Sprout Project and in part by S.H.T.'s research fundings, both of which are granted by the Ministry of Education (109L9006 and 110L891502) and the Ministry of Science and Technology in Taiwan (MOST 109-2221-E-002-182-MY3, 110-2634-F-002-043, 108-2923-E-002-001-MY3, and 110-2622-8-007-015).

■ REFERENCES

(1) Xue, J.; Wu, T.; Dai, Y.; Xia, Y. Electrospinning and Electrospun Nanofibers: Methods, Materials, and Applications. *Chem. Rev.* **2019**, *119*, 5298−5415.

(2) Huang, C.; Thomas, N. L. Fabrication of porous fibers via electrospinning: strategies and applications. *Polym. Rev.* **2020**, *60*, 595−647.

(3) Zaarour, B.; Zhu, L.; Jin, X. A Review on the Secondary Surface Morphology of Electrospun Nanofibers: Formation Mechanisms, Characterizations, and Applications. *ChemistrySelect* **2020**, *5*, 1335−1348.

(4) Chang, H.-H.; Beltsios, K.; Chen, Y.-H.; Lin, D.-J.; Cheng, L.-P. Effects of Cooling Temperature and Aging Treatment on the Morphology of Nano- and Micro-Porous Poly(ethylene-co-vinyl alcohol) Membranes by Thermal Induced Phase Separation Method. *J. Appl. Polym. Sci.* **2014**, *131*, 40374.

(5) Ye, X.-Y.; Lin, F.-W.; Huang, X.-J.; Liang, H.-Q.; Xu, Z.-K. Polymer fibers with hierarchically porous structure: combination of high temperature electrospinning and thermally induced phase separation. *RSC Adv.* **2013**, *3*, 13851−13858.

(6) McCann, J. T.; Marquez, M.; Xia, Y. Highly Porous Fibers by Electrospinning into a Cryogenic Liquid. *J. Am. Chem. Soc.* **2006**, *128*, 1436−1437.

(7) Zheng, J.; Zhang, H.; Zhao, Z.; Han, C. C. Construction of hierarchical structures by electrospinning or electrospraying. *Polymer* **2012**, *53*, 546−554.

(8) Megelski, S.; Stephens, J. S.; Chase, D. B.; Rabolt, J. F. Micro- and Nanostructured Surface Morphology on Electrospun Polymer Fibers. *Macromolecules* **2002**, *35*, 8456−8466.

(9) Wu, J.; Wang, N.; Wang, L.; Dong, H.; Zhao, Y.; Jiang, L. Electrospun Porous Structure Fibrous Film with High Oil Adsorption Capacity. *ACS Appl. Mater. Interfaces* **2012**, *4*, 3207−3212.

(10) Nezarati, R. M.; Eifert, M. B.; Cosgriff-Hernandez, E. Effects of Humidity and Solution Viscosity on Electrospun Fiber Morphology. *Tissue Eng., Part C* **2013**, *19*, 810−819.

(11) Casper, C. L.; Stephens, J. S.; Tassi, N. G.; Chase, D. B.; Rabolt, J. F. Controlling Surface Morphology of Electrospun Polystyrene Fibers: Effect of Humidity and Molecular Weight in the Electrospinning Process. *Macromolecules* **2004**, *37*, 573−578.

(12) Tian, R.; Zhang, P.; Lv, R.; Na, B.; Liu, Q.; Ju, Y. Formation of highly porous structure in the electrospun polylactide fibers by swelling-crystallization in poor solvents. *RSC Adv.* **2015**, *5*, 37539−37544.

(13) Seo, Y.-A.; Pant, H. R.; Nirmala, R.; Lee, J.-H.; Song, K. G.; Kim, H. Y. Fabrication of highly porous poly (epsilon-caprolactone) microfibers via electrospinning. *J. Porous Mater.* **2012**, *19*, 217−223.

(14) Nayani, K.; Katepalli, H.; Sharma, C. S.; Sharma, A.; Patil, S.; Venkataraghavan, R. Electrospinning Combined with Nonsolvent-Induced Phase Separation To Fabricate Highly Porous and Hollow Submicrometer Polymer Fibers. *Ind. Eng. Chem. Res.* **2012**, *51*, 1761−1766.

(15) Huang, C.; Thomas, N. L. Fabricating porous poly(lactic acid) fibres via electrospinning. *Eur. Polym. J.* **2018**, *99*, 464−476.

(16) Wei, Z.; Zhang, Q.; Wang, L.; Wang, X.; Long, S.; Yang, J. Porous Electrospun Ultrafine Fibers via a Liquid−liquid Phase Separation Method. *Colloid Polym. Sci.* **2013**, *291*, 1293−1296.

(17) Qi, Z.; Yu, H.; Chen, Y.; Zhu, M. Highly Porous Fibers Prepared by Electrospinning a Ternary System of Nonsolvent/Solvent/Poly(L-lactic acid). *Mater. Lett.* **2009**, *63*, 415−418.

(18) Katsogiannis, K. A. G.; Vladisavljević, G. T.; Georgiadou, S. Porous Electrospun Polycaprolactone (PCL) Fibres by Phase Separation. *Eur. Polym. J.* **2015**, *69*, 284−295.

(19) Stodolak-Zych, E.; Dzierzkowska, E.; Matwally, S.; Mikołajczyk, M.; Gajek, M.; Rapacz-Kmita, A. Multifunctional porous membranes with antibacterial properties. *Int. J. Polym. Mater. Polym. Biomater.* **2019**, *68*, 19−26.

(20) Rezabeigi, E.; Sta, M.; Swain, M.; McDonald, J.; Demarquette, N. R.; Drew, R. A. L.; Wood-Adams, P. M. Electrospinning of porous polylactic acid fibers during nonsolvent induced phase separation. *J. Appl. Polym. Sci.* **2017**, *134*, 44862.

(21) Şimşek, M. Tuning surface texture of electrospun polycaprolactone fibers: Effects of solvent systems and relative humidity. *J. Mater. Res.* **2020**, *35*, 332−342.

(22) Srinivasarao, M.; Collings, D.; Philips, A.; Patel, S. Three-Dimensionally Ordered Array of Air Bubbles in a Polymer Film. *Science* **2001**, *292*, 79−83.

(23) Natarajan, L.; New, J.; Dasari, A.; Yu, S.; Manan, M. A. Surface morphology of electrospun PLA fibers: mechanisms of pore formation. *RSC Adv.* **2014**, *4*, 44082−44088.

(24) Lu, P.; Xia, Y. Maneuvering the Internal Porosity and Surface Morphology of Electrospun Polystyrene Yarns by Controlling the Solvent and Relative Humidity. *Langmuir* **2013**, *29*, 7070−7078.

(25) Bognitzki, M.; Czado, W.; Frese, T.; Schaper, A.; Hellwig, M.; Steinhart, M.; Greiner, A.; Wendorff, J. H. Nanostructured fibers via electrospinning. *Adv. Mater.* **2001**, *13*, 70−72.
(26) Liang, Y.; Lin, C.; Guan, J.; Li, Y. Silver nanoparticle-immobilized porous POM/PLLA nanofibrous membranes: efficient catalysts for reduction of 4-nitroaniline. *RSC Adv.* **2017**, *7*, 7460−7468.
(27) Cui, W.; Li, X.; Zhou, S.; Weng, J. Degradation patterns and surface wettability of electrospun fibrous mats. *Polym. Degrad. Stab.* **2008**, *93*, 731−738.
(28) Bognitzki, M.; Frese, T.; Steinhart, M.; Greiner, A.; Wendorff, J. H.; Schaper, A.; Hellwig, M. Preparation of fibers with nanoscaled morphologies: Electrospinning of polymer blends. *Polym. Eng. Sci.* **2001**, *41*, 982−989.
(29) Gupta, A.; Saquing, C. D.; Afshari, M.; Tonelli, A. E.; Khan, S. A.; Kotek, R. Porous Nylon-6 Fibers via a Novel Salt-Induced Electrospinning Method. *Macromolecules* **2009**, *42*, 709−715.
(30) Chen, J.-T.; Chen, W.-L.; Fan, P.-W. Hierarchical Structures by Wetting Porous Templates with Electrospun Polymer Fibers. *ACS Macro Lett.* **2012**, *1*, 41−46.
(31) Chen, P.-Y.; Tung, S.-H. One-Step Electrospinning To Produce Nonsolvent-Induced Macroporous Fibers with Ultrahigh Oil Adsorption Capability. *Macromolecules* **2017**, *50*, 2528−2534.
(32) El-Samak, A. A.; Ponnamma, D.; Hassan, M. K.; Adham, S.; Karim, A.; Ammar, A.; Alser, M.; Shurbaji, S.; Eltai, N. O.; Al-Maadeed, M. A. A. Multifunctional Oil Absorption with Macroporous Polystyrene Fibers Incorporating Silver-Doped ZnO. *ACS Omega* **2021**, *6*, 8081−8093.
(33) Li, Y.; Lim, C. T.; Kotaki, M. Study on structural and mechanical properties of porous PLA nanofibers electrospun by channel-based electrospinning system. *Polymer* **2015**, *56*, 572−580.
(34) Deng, Y.-F.; Zhang, D.; Zhang, N.; Huang, T.; Lei, Y.-Z.; Wang, Y. Electrospun stereocomplex polylactide porous fibers toward highly efficient oil/water separation. *J. Hazard. Mater.* **2021**, *407*, 124787.
(35) Zhang, D.; Jin, X.-Z.; Huang, T.; Zhang, N.; Qi, X.-d.; Yang, J.-h.; Zhou, Z.-w.; Wang, Y. Electrospun Fibrous Membranes with Dual-Scaled Porous Structure: Super Hydrophobicity, Super Lipophilicity, Excellent Water Adhesion, and Anti-Icing for Highly Efficient Oil Adsorption/Separation. *ACS Appl. Mater. Interfaces* **2019**, *11*, 5073−5083.
(36) Liang, J.-W.; Prasad, G.; Wang, S.-C.; Wu, J.-L.; Lu, S.-G. Enhancement of the Oil Absorption Capacity of Poly(Lactic Acid) Nano Porous Fibrous Membranes Derived via a Facile Electrospinning Method. *Appl. Sci.* **2019**, *9*, 1014.
(37) Xue, Z.; Sun, Z.; Cao, Y.; Chen, Y.; Tao, L.; Li, K.; Feng, L.; Fu, Q.; Wei, Y. Superoleophilic and superhydrophobic biodegradable material with porous structures for oil absorption and oil-water separation. *RSC Adv.* **2013**, *3*, 23432−23437.
(38) Zhang, D.; Zhang, N.; Ma, F.-f.; Qi, X.-d.; Yang, J.-h.; Huang, T.; Wang, Y. One-step fabrication of functionalized poly(L-lactide) porous fibers by electrospinning and the adsorption/separation abilities. *J. Hazard. Mater.* **2018**, *360*, 150−162.
(39) Gu, J.; Xiao, P.; Chen, P.; Zhang, L.; Wang, H.; Dai, L.; Song, L.; Huang, Y.; Zhang, J.; Chen, T. Functionalization of Biodegradable PLA Nonwoven Fabric as Superoleophilic and Superhydrophobic Material for Efficient Oil Absorption and Oil/Water Separation. *ACS Appl. Mater. Interfaces* **2017**, *9*, 5968−5973.
(40) Song, J.; Zhang, B.; Lu, Z.; Xin, Z.; Liu, T.; Wei, W.; Zia, Q.; Pan, K.; Gong, R. H.; Bian, L.; Li, Y.; Li, J. Hierarchical Porous Poly(L-lactic acid) Nanofibrous Membrane for Ultrafine Particulate Aerosol Filtration. *ACS Appl. Mater. Interfaces* **2019**, *11*, 46261−46268.
(41) Thorvaldsson, A.; Stenhamre, H.; Gatenholm, P.; Walkenström, P. Electrospinning of highly porous scaffolds for cartilage regeneration. *Biomacromolecules* **2008**, *9*, 1044−1049.
(42) Washburn, E. W. The dynamics of capillary flow. *Phys. Rev.* **1921**, *17*, 273−283.
(43) Li, H.; Li, Y.; Yang, W.; Cheng, L.; Tan, J. Needleless Melt-Electrospinning of Biodegradable Poly(Lactic Acid) Ultrafine Fibers for the Removal of Oil fromWater. *Polymers* **2017**, *9*, 3.

https://doi.org/10.1021/acsapm.1c00855
ACS Appl. Polym. Mater. 2021, 3, 5096−5104